Mechanism of hollow-core-fiber infrared-supercontinuum compression with bulk material

P. Béjot,[1,*] B. E. Schmidt,[2,†] J. Kasparian,[3] J.-P. Wolf,[3] and F. Legaré[2]

[1]*Laboratoire Interdisciplinaire CARNOT de Bourgogne, UMR 5209 CNRS-Université de Bourgogne, BP 47870, F-21078 Dijon Cedex, France*

[2]*Institut National de la Recherche Scientifique, Centre Énergie Matériaux et Télécommunications, 1650 Boulevard Lionel-Boulet, Varennes, Québec J3X1S2, Canada*

[3]*GAP-Biophotonics, Université de Genève, 20 rue de l'École de Médecine, CH-1211 Geneva 4, Switzerland*

(Received 23 March 2010; published 28 June 2010)

We numerically investigate the pulse compression mechanism in the infrared spectral range based on the successive action of nonlinear pulse propagation in a hollow-core fiber followed by linear propagation through bulk material. We found an excellent agreement of simulated pulse properties with experimental results at 1.8 μm in the two-optical-cycle regime close to the Fourier limit. In particular, the spectral phase asymmetry attributable to self-steepening combined with self-phase modulation is a necessary prerequisite for subsequent compensation by the phase introduced by glass material in the anomalous dispersion regime. The excellent agreement of the model enabled simulating pressure and wavelength tunability of sub-two cycles in the range from 1.5 to 4 μm with this cost-efficient and robust approach.

DOI: 10.1103/PhysRevA.81.063828 PACS number(s): 42.65.Re, 42.65.Jx

I. INTRODUCTION

The ability to study molecular dynamics was one motivation to improve chirped pulse amplification (CPA) [1] in terms of reduced pulse duration and increased energy since the early 1990s. The key ingredient for reducing the pulse duration to few optical cycles at high power levels lies in additional spectral broadening through either (i) nonlinear propagation in hollow-core-fiber (HCF) [2] and laser-induced (co-)filaments [3–5] or (ii) ultrabroadband optical parametric amplification (OPA) [6] and OPCPA [7]. However, the main challenge remains in controlling the spectral phase of the ultrabroadband spectrum. Conventional prism or grating configurations have been demonstrated for pulse compression to few optical cycles. However, prisms suffer from higher-order distortions and nonlinear effects at high peak powers, while gratings introduce losses. Active devices such as spatial light modulators offer full control over the spectral phase but are elaborate experimentally [8] and also induce high losses. The established state of the art for high-power, carrier-envelope phase (CEP), stable, few-cycle pulse generation consists of chirped mirrors typically being used subsequently to induce broadening in a HCF.

Based on those achievements at 800 nm wavelength, the development of attosecond technology in the framework of high-order harmonic generation (HHG) during the past decade accessed a previously unexplored time scale down to currently 80 as [9]. Because the extension of the XUV spectrum scales as $I\lambda^2$ [10,11], reliable sources delivering high intensities I at longer wavelengths λ of the driving laser are required to generate shorter attosecond pulses. The present article numerically investigates the mechanism of a cost-efficient approach for compression of intense IR few-cycle pulses that has been recently demonstrated experimentally [12]. This technique is based on spectral broadening in an argon-filled HCF followed by compression using anomalous dispersion of fused silica (FS) which introduces negative group delay dispersion (GDD) in this IR spectral range. The motivation of the present numerical study is to explain why the compression is not limited by third-order dispersion (TOD), which is positive for all materials. By the help of one-dimensional propagation simulations, we identified the exact compression mechanism. The action in argon of the Kerr effect up to the 10th order combined with dispersion and self-steepening generates a spectral asymmetry whose phase is adequately opposed to the one subsequently introduced by linear anomalous propagation through FS. Note that this technique differs from [13], where the propagation inside the output window has to be nonlinear to compress the pulse after the propagation cell.

II. EXPERIMENTAL AND NUMERICAL METHODS

The experimental setup employed to demonstrate the new compression concept [12] is depicted in Fig. 1. It shows the IR source which is a fluorescence-seeded, high-energy OPA (HE-TOPAS, Light Conversion) pumped by 7-mJ, 40-fs pulses from a Ti:Sa CPA. The OPA Idler wavelength is tuned to 1.83 μm providing a pulse duration of 73 fs and 0.93 mJ of pulse energy. The IR laser beam is coupled to a HCF (400 μm in diameter, 1.4 bar argon pressure) using a $f = 1$-m plano-convex lens. Lens and cell windows are made of CaF_2 to introduce minimal dispersion to the OPA pulses. Due to Fresnel losses on the uncoated glass surfaces, approximately 0.82 mJ is coupled into the fiber. The pure fiber transmission is estimated to be 65% and the output beam is collimated using an $R = 2$-m concave silver mirror. Pulses are then recompressed by a single pass through a 3-mm FS glass plate. Their characterization is carried out with a home-built second-harmonic-generation–frequency-resolved optical gating (SHG-FROG) specially designed for few-cycle pulse measurement [14]. The experimental data appear as red circles in Fig. 2 as a reference for the numerical simulations (solid blue curve). Figure 2(a) shows the broadened spectra after the HCF with its corresponding spectral phase before compensation by the FS plate in (c). On the other hand, the spectral phase in (d) includes the contribution of nonlinear propagation in the fiber plus the linear propagation through FS in the

*pierre.bejot@u-bourgogne.fr
†schmidtb@emt.inrs.ca

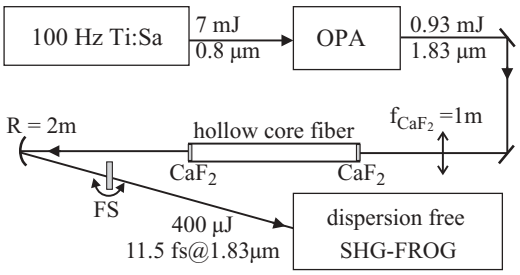

FIG. 1. Experimental setup. Idler pulses from a high-energy OPA are propagated in a hollow-core fiber filled with 1.4 bar argon. The broadband pulses are subsequently compressed by linear propagation through a fused silica (FS) plate of 3 mm thickness.

anomalous dispersion regime. Experimentally, this flat phase is determined by varying the glass thickness by steps of 0.5 mm and small angular tilts, which lead to the generation of 11.5-fs pulses displayed in Fig. 2(b). This excellent compression to only 1.14 times the FL (10.1 fs) is surprising even though the GDD of FS is negative in the anomalous dispersion regime. As discussed in [12], the TOD, which is positive for all gases, would be expected to broaden a FL pulse to almost 15 fs (1.5 times the FL) after passing the FS and CaF_2 if it was the only process in play.

To bring insight into the compression mechanism, we precisely modeled the nonlinear propagation in the HCF, as well as the linear propagation through the glass, according to the experimental conditions. Let us consider a linearly polarized incident electric field $E = \mathrm{Re}\,e\{\varepsilon(z,t)\exp[i(k_0 z - \omega_0 t)]\}$ at wavelength $\lambda_0 = 1.83$ μm traveling in a HCF filled with argon along the propagation axis z. $k_0 = 2\pi n_0/\lambda_0$ and $\omega_0 = 2\pi c/\lambda_0$ are the wave number and the frequency of the carrier wave, respectively. The refractive index n is evaluated according to the Sellmeier equation of argon at 1 bar [15] and its pressure dependence is given by

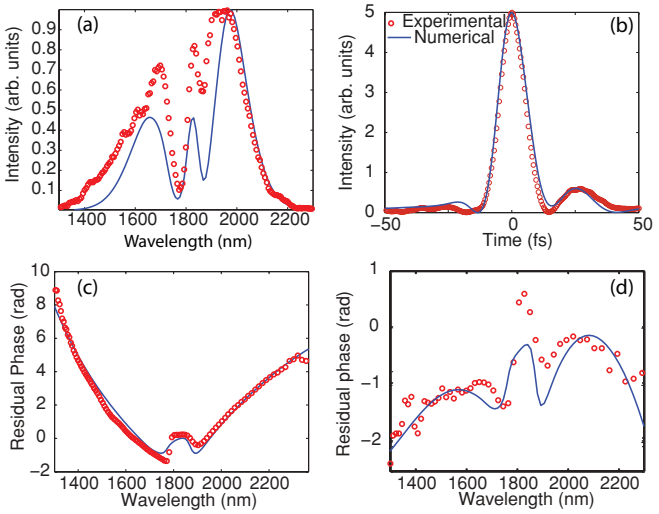

FIG. 2. (Color online) Comparison between experimental (red circles) and theoretical (solid blue line) results. (a) Power spectrum for propagation in argon at pressure of 1.4 bar, (c) spectral phase of the pulse before and (d) after compensation with 3-mm FS. The temporal intensity profile of the compressed pulse is shown in (b).

TABLE I. Nonlinear indexes of argon at 1.83 μm used in the model (p accounts for the relative gas pressure: $p = \frac{P}{1\,\mathrm{bar}}$). α accounts for the fiber optical losses.

n_2	n_4	n_6	n_8	n_{10}	α
10^{-24}	10^{-42}	10^{-58}	10^{-75}	10^{-94}	
$\mathrm{m^2\,W^{-1}}$	$\mathrm{m^4\,W^{-2}}$	$\mathrm{m^6\,W^{-3}}$	$\mathrm{m^8\,W^{-4}}$	$\mathrm{m^{10}\,W^{-5}}$	$\mathrm{m^{-1}}$
$9.73p$	$-3.55p$	$3.78p$	$-1.59p$	$8.10p$	$0.43p$

$n(p) = \sqrt{1 + p[n(p=1)^2 - 1]}$, where $p = P/1$ bar accounts for the relative pressure. The scalar envelope $\varepsilon(r,t,z)$ is assumed to be slowly varying in time and along z. In the frequency domain, it therefore evolves according to the nonlinear Schrödinger equation (NLSE) [16],

$$\partial_z \widetilde{\varepsilon} = \widetilde{D}\widetilde{\varepsilon} + ik_0 T\widetilde{\Delta n}\varepsilon - \frac{\widetilde{\alpha}}{2}\widetilde{\varepsilon}, \tag{1}$$

where $\widetilde{\varepsilon}$ is the Fourier transform of ε. The terms on the right-hand side of Eq. (1) account for dispersion [$\widetilde{D}(\omega) = k(\omega) - k_0 - k_1(\omega - \omega_0)$], self-steepening ($T = 1 + i\tau_{\mathrm{shock}}\partial_t$, where $\tau_{\mathrm{shock}} \simeq 1/\omega_0$), instantaneous Kerr effects ($\Delta n = \sum_{m=1}^{5} n_{2m}|\varepsilon|^{2m}$ includes the contribution of higher nonlinear indexes up to n_{10}), and optical losses α. The n_{2m} coefficients are related to $\chi^{(2m+1)}$ susceptibilities and have been reported in a recent article [17] at 800 nm. We then extrapolated these indexes at 1.83 μm by using generalized Miller formulas [18], providing the spectral dependence of the n_{2m} coefficients from the knowledge of the linear dispersion. The calculated nonlinear refractive indexes used in this article are summarized in Table I. Losses α have been estimated from the experimental measurements described in [12]. Equation (1) is valid even for subcycle pulses [19]. Finally, we numerically checked that ionization does not play a role in the process. According to PPT theory, the plasma density for the considered intensities is lower than 10^{11} $\mathrm{cm^{-3}}$, inducing a refractive index change four orders lower than the Kerr-induced one.

The input electric field envelope is modeled by a Gaussian profile as

$$\varepsilon(t,0) = \sqrt{\frac{2P_{\mathrm{in}}}{\pi\sigma_r^2}}\exp\left(-\frac{t^2}{\sigma_t^2}\right), \tag{2}$$

where P_{in} denotes for the initial peak power, σ_r is the intensity quadratic radius, and $\sigma_t = \Delta t_{\mathrm{FWHM}}/\sqrt{2\ln(2)}$ (Δt_{FWHM} is the full width at half maximum of temporal intensity). P_{in} is then calculated as $P_{\mathrm{in}} = \sqrt{\frac{2}{\pi}}\frac{E_{\mathrm{in}}}{\sigma_t}$, E_{in} being the pulse energy. The initial conditions are chosen to match the experimental parameters of [12], as summarized in Table II.

Equation (1) is solved with a split-step Fourier algorithm for 1 m fiber length. At each propagation step, the dispersion terms are computed in the frequency domain, whereas both the nonlinear contributions and the self-steepening are treated

TABLE II. Initial conditions used in the model, corresponding to the experiments driven in [12].

E_{in} (mJ)	Δt_{FWHM} (fs)	σ_r (μm)	P_{in} (GW)
0.82	73	210	10.5

in the time domain. The self-steepening is solved by using a second-order Runge-Kutta procedure. Moreover, we ensured that increasing the temporal resolution does not change our numerical results.

In order to reproduce experimental conditions, we then apply the spectral phase function induced by both the 1-mm CaF_2 output window and the FS plates with different thicknesses. This function is calculated according to the Sellmeier equations giving the spectral dependence of the CaF_2 and FS refractive indexes [20,21]. In addition, we checked experimentally that no spectral broadening occurs when the fiber is empty, that is, the propagation within the CaF_2 plates remains linear.

III. RESULTS AND DISCUSSION

Figure 2 compares the experimental and numerical results at a glance. It displays the broadened power spectrum after nonlinear propagation (a), the corresponding spectral phase before (c) and after (d) compression with 3 mm FS. Measured and simulated temporal intensities after compression are shown in (b). The crucial task of the numerical work was to determine the origin for the asymmetry of (i) the spectral shape in (a) and (ii) the phase which is then efficiently compensated by glass material in the anomalous dispersion regime shown in (d). The excellent match for nonlinear propagation according to the full model given by Eq. (1) and subsequent compression with bulk material revealed that SPM, self-steepening, and higher-order Kerr terms during propagation in the fiber are the three relevant nonlinear effects for describing the experimental observations. The aim of the current section is to discuss their respective contributions to the final compression with a simple FS plate. We stress the fact that simulations match exactly experimental conditions. The low peak power of 10.5 GW, which is less than one-third the critical power for self-focusing in argon (≈37 GW at 1.4 bar), prevents spatiotemporal pulse collapse and thus fully justifies the 1D + 1 modeling.

A. Pulse compression to few optical cycles

Before having a closer look at the details of the nonlinear propagation, we numerically describe the compression by linear propagation through a bulk material in the anomalous dispersion regime. Due to self-steepening, the asymmetric spectral shape of Fig. 2(a) is accompanied by an asymmetric spectral phase. This uncompensated phase after the fiber assembly but before the FS plate is shown in Fig. 3(a) as a red line. In the temporal domain it causes the trailing edge to be more abrupt than the leading one, producing a strong asymmetry in the temporal intensity profile plotted in Fig. 3(b). Its FWHM pulse duration is about 75 fs after the CaF_2 window, close to the 68 fs measured experimentally but far longer than the FL of 11.3 fs. Obviously, the output spectral phase is predominantly positively chirped, as expected from SPM-induced broadening. Pure SPM induces a spectral phase that is typically approximated by a quadratic function and therefore can be compensated because the GDD of both FS and CaF_2 is negative in the anomalous dispersion regime. Thus, a pulse which has experienced Kerr-induced spectral broadening can be temporally compressed by travel through an adequate

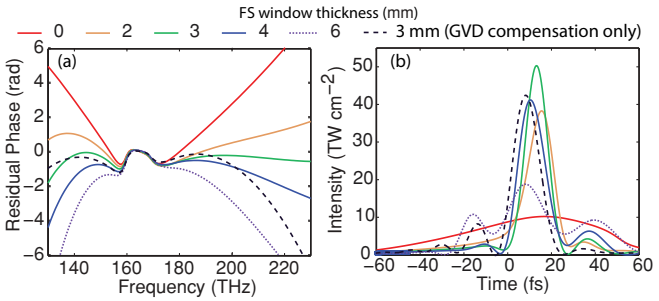

FIG. 3. (Color online) Pulse compression for the spectrum of Fig. 2 by adding different amounts of FS. The color coding for the spectral phases in (a) corresponds to the temporal intensities in (b). Comparing the green with the black dashed plot demonstrates the effect of uncompensated TOD components.

FS plate, as depicted in Fig. 3. The figure illustrates the effect of different glass thicknesses on the spectral phase and corresponding time profile whereby the complete phase introduced by FS is calculated according to the Sellmeier equation. The best compression is obtained using a 2.77-mm FS plate and leads to a pulse duration of 10.9 fs, which corresponds to about 1.8 optical cycles at 1.83 μm. Moreover, we calculated that using a 3-mm FS plate leads to a pulse duration of 11.1 fs. The agreement is excellent, even quantitatively, since the shortest experimentally measured duration was 11.5 fs along with a FL of 10.1 fs. Moreover, the contrast between the main pulse and satellite pulses remains relatively high (about 11), in both experiment and simulation. However, this situation worsens if only the GDD is compensated for. To demonstrate this, we calculated compression taking into account only the negative GDD of 3-mm FS instead of taking the full Sellmeier formula into account (short-dashed line in Fig. 3). Apparently, the compression cannot reach the FL mainly because of remaining higher-order dispersion, which is not fully compensated by FS, as depicted in Fig. 3(a). That means if the negative TOD component after nonlinear propagation is not compensated by the bulk material, the pulse duration increases to 13.5 fs.

B. Mechanism study: Respective contributions of the processes in play

Starting from the initial conditions summarized in Table II the nonlinear propagation was simulated investigating different nonlinear effects. As expected, the third-order Kerr term (n_2 in Table I), typically referred to as SPM, is the driving force for spectral broadening [16]. After 1 m of propagation the broadened spectrum symmetrically spans over 1 μm (from 1.3 to 2.3 μm), as can be seen in Fig. 4(a). Even though spectral bandwidth and FL pulse durations are comparable with those of the experiment, the spectral shape and phase are not adequately reproduced (data not shown). On the other hand, the full model corresponding to the solid line in Fig. 2 including self-steepening and higher-order Kerr terms exhibits different propagation dynamics, as illustrated in Fig. 4(b), and yields remarkable agreement with the experiment result.

To track the contribution of different nonlinear effects, we successively introduced them in the numerical model and compare the corresponding outcomes. Table III summarizes the characteristic lengths L_x of all processes taken into

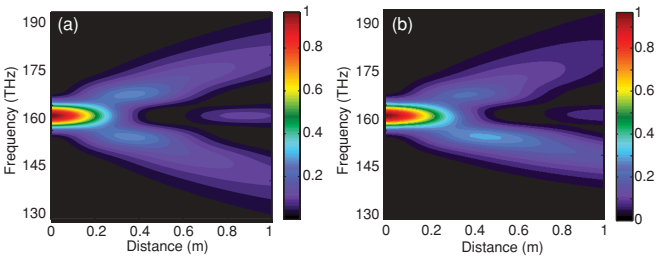

FIG. 4. (Color online) Spectral evolution as a function of propagation distance for the simple case considering only n_2 in (a) and for the full model in (b). The latter clearly resembles an asymmetry because of self-steepening, which tends to promote the higher-frequency region.

account. As expected, the main process driving the pulse propagation (i.e., the process with the shortest characteristic length) is the total Kerr effect, whereas the gas dispersion remains negligible. As shown in [22], even if the first order remains most important during the propagation, it appears that the higher-order Kerr contributions have a non-negligible effect, leading to a refractive index saturation at an intensity of 19 TW cm^{-2} and even a negative nonlinear refractive index for intensities higher than 27 TW cm^{-2}.

Moreover, as depicted in Table III, self-steepening is not the main process driving the pulse propagation since its characteristic length $L_{\text{steepening}}$ is about 50 times longer than those of the Kerr effect. In any case, since $L_{\text{steepening}}$ is comparable with the fiber length, it cannot be neglected. In that section, we investigate how the steepening modifies the final result, and in particular the compression.

As mentioned earlier, the simple case of pure SPM, which only takes into account the first-order Kerr term, is not appropriate for explaining the results of Fig. 2. To find the nonlinear pulse-shaping mechanism that allows for subsequent compression with bulk material, we investigate the effect of the following three models:

(i) Kerr model: Includes higher-order Kerr effects but without self-steepening (green dashed-dotted line in Fig. 5);

(ii) Reduced model: Includes only the third-order Kerr effect and self-steepening (dashed blue line in Fig. 5);

(iii) Full model: Includes higher-order (up to 11th) Kerr terms and self-steepening (red solid line in Fig. 5).

TABLE III. Characteristic lengths of the different processes taking place during the propagation.

Nonlinear effect	Characteristic length	Distance (m)
Kerr (3rd order)	$\lvert c/(\omega_0 n_2 \lvert\varepsilon\rvert^2)\rvert$	0.136
Kerr (5th order)	$\lvert c/(\omega_0 n_4 \lvert\varepsilon\rvert^4)\rvert$	2.38
Kerr (7rd order)	$\lvert c/(\omega_0 n_6 \lvert\varepsilon\rvert^6)\rvert$	0.142
Kerr (9th order)	$\lvert c/(\omega_0 n_8 \lvert\varepsilon\rvert^8)\rvert$	0.217
Kerr (11th order)	$\lvert c/(\omega_0 n_{10} \lvert\varepsilon\rvert^{10})\rvert$	2.7
Kerr (full)	$\lvert c/(\omega_0 \sum_{m=1}^{5} n_{2m} \lvert\varepsilon\rvert^{2m})\rvert$	0.112
Self-steepening	$\lvert c\sigma_t/(\sum_{m=1}^{5} n_{2m} \lvert\varepsilon\rvert^{2m})\rvert$	5
Dispersion	$\lvert\sigma_t^2/k^{(2)}\rvert$	156

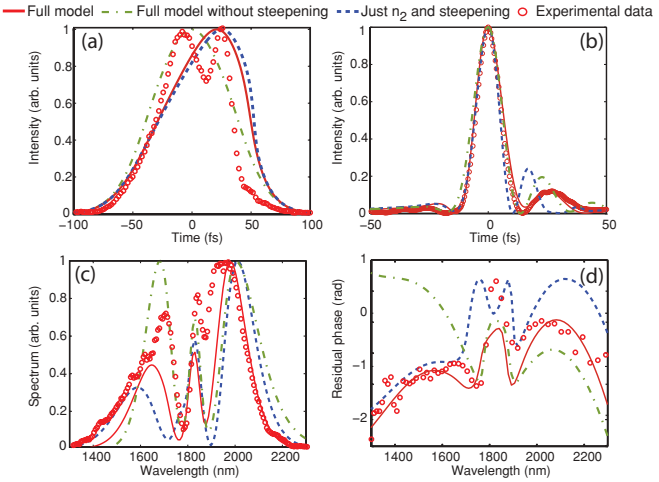

FIG. 5. (Color online) Comparison of the three numerical models with experimental measurements. (a,b) Time profile of (a) the uncompressed and (b) the compressed pulses. (c) Broadened power spectrum and (d) its associated phase when the pulse is compressed.

Above all, one can see that using the pure Kerr model is not sufficient for accurately describing the output spectral shape or its phase. In particular, it is obvious from Fig. 5(d) that the phase in the blue part of the spectrum strongly deviates from the experiment. This also reflects as a longer pulse duration of 12.9 fs and a reduced contrast ratio between main and satellite pulses.

Accounting for self-steepening is the key advance of the reduced model (blue line), which enables modeling an asymmetric spectral shape and phase being much closer to the experimental one than the the Kerr model. However, small discrepancies of the spectral peak positions in combination with additional phase modulations around the center wavelength lead to an enhanced postpulse appearing at shorter delay than that seen in the experiment.

For the considered experimental conditions, the full model describes the broadening process to a much higher degree of accurateness, as is evident when comparing the result with experimental data. The spectral shape, both compressed and uncompressed phase, as well as the temporal intensity, match perfectly except for a small deviation of the blue spectral peak in the 1400- to 1700-nm spectral range. The relative peak height and the cutoff on the blue side are reduced. The latter might explain a slightly longer FL of 10.8 fs in the simulation compared to the 10.1 fs in the experiment. However, the phase in the same region agrees very well and so does the temporal appearance of main and satellite pulses.

Residual discrepancies could originate from the approximation in the steepening term $\tau_{\text{shock}} \simeq \frac{1}{\omega_0}$. In particular, it has been demonstrated that for quite a broad spectrum τ_{shock} has to be corrected as $\tau_{\text{shock}} = \frac{1}{\omega_0} - \frac{\partial \ln[A_{\text{eff}}(\omega)]}{\partial\omega}|_{\omega_0}$ [23], where $A_{\text{eff}}(\omega)$ is the effective area. This correction induces a change in the spectrum asymmetry and could indeed explain the difference between experiments and numerical results in Fig. 5. Moreover, spatiotemporal couplings which intrinsically cannot be taken into account in 1D simulations or excitation of higher-order transverse modes cannot be totally ruled out for explaining these discrepancies.

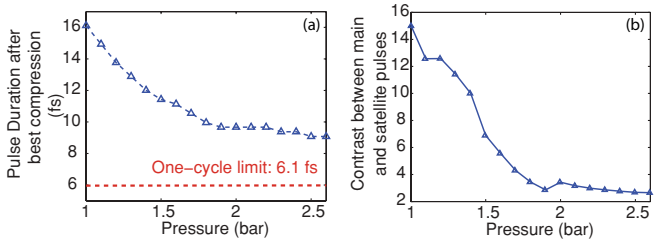

FIG. 6. (Color online) Pressure dependence of (a) minimal pulse duration achievable by compression with optimized FS thickness in each case and (b) ratio between main and satellite pulse intensities.

However, this correction does not affect the bottom line of the numerical investigations. Our results prove that neglecting self-steepening leads to underestimating the compression efficiency (the best compression gives 12.9 fs, that is, 2.1 cycles) and the contrast between the main and the satellite pulses (about 5), indicating that self-steepening induces an opposite contribution to the positive TOD of the FS plate. Moreover, as in [22], it appears that the higher-order Kerr terms have to be included in order to quantitatively reproduce experiments.

C. Parameters dependence

Enforced by the quantitative agreement of our full model, we performed a parameter study in order to find the optimal conditions to generate single-cycle IR pulses with a clean temporal shape (i.e., without any post- or prepulses). In that regard, we investigate how the compression behaves as functions of both wavelength and argon pressure. Adjusting the pressure is a very handy method for controlling the spectral broadening, simply because n_2 is proportional to the pressure. Indeed, a higher pressure is expected to broaden the spectrum even more, leading in turn to shorter compressed pulses, provided an adequate FS plate can compensate for potentially more complex spectral phases induced by both SPM and self-steepening as the pulse spectrum gets broader and broader. In addition, when aiming for even shorter XUV attosecond pulses, few-cycle driving fields in the IR region are strongly desirable simply because the extension of the XUV spectrum is proportional to the kinetic energy of the accelerated electron scaling as $I\lambda^2$. In that framework, we have extended our analysis to longer wavelengths, and

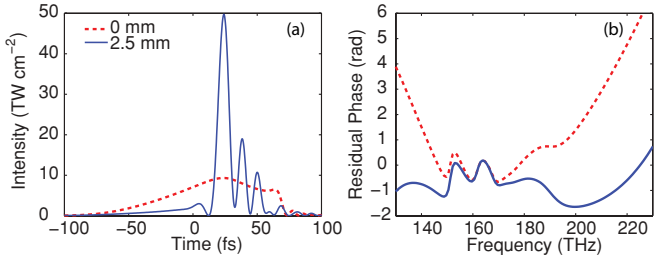

FIG. 7. (Color online) (a) Temporal profile and (b) residual spectral phase of the pulse for a pressure of 2.6 bar without (dashed red line) and with (blue line) the best compression leading to a FWHM duration of 1.25 cycles.

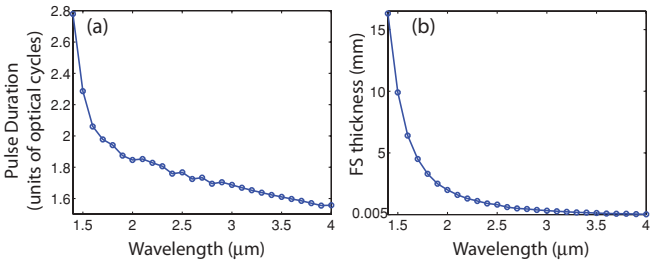

FIG. 8. (Color online) (a) Temporal duration (in cycle units) at different wavelengths of pulses compressed with an optimal FS thickness. The best FS thicknesses are displayed in (b). Note that the CaF_2 exit window is taken into account.

we discuss the efficiency of the method to generate single-cycle pulses in the 1.4- to 4-μm spectral region.

1. Pressure dependence at 1.83 μm

We first performed calculations as a function of pressure according to the experimental conditions (i.e., setting the other parameters like in the experimental conditions being discussed in the first section). As depicted in Fig. 6(a), a higher pressure leads to a shorter main pulse, however, at the cost of the growth of satellite pulses in the trailing edge of the pulse [see Fig. 6(b)]. For instance, the best compression with a FS plate at a pressure of 2.6 bar is about 7.5 fs, which is less than 1.25 cycles. However, as depicted in Fig. 7, the nonlinear induced spectral phase cannot be fully compensated by the FS plate, causing the birth of several satellite pulses. Moreover, increasing the pressure above 2.6 bar enhances those satellite pulses without reducing the main pulse duration. In other words, a trade-off between the pulse duration and contrast of main and satellite pulses has to be accepted due to uncompensated higher-order dispersion.

2. Wavelength dependence at 1.4 bar pressure

In this section, we describe how the compression behaves as the pulse central wavelength is varied for all other parameters, keeping the same initial conditions of the first section. Figure 8(a) displays the pulse duration as a function of the pulse central wavelength and shows the scalability for generating sub-two-cycle pulses with this very simple compression technique at least from 1.7 to 4 μm. Nevertheless, as depicted in Fig. 8, the compression ability below 1.7 μm diminishes, mainly because the zero second-order dispersion wavelength lies at around 1.3 μm. On the contrary, the ratio k_2/k_3 of FS being higher at longer wavelengths, the propagation through the FS plate leads in turn to a better compression at longer central wavelengths. However, since the nonlinear refractive index n_2 decreases as the wavelength increases and since the same B integral [$B = n_2 \int_0^L I(z)\, dz$] has to be accumulated to obtain an equivalent spectral broadening, it appears that the compression at longer wavelengths is limited at this pressure mainly because of the limited spectral broadening.

IV. CONCLUSION

In this article, we have identified the mechanisms allowing for pulse compression of IR pulses in a FS plate after

spectral broadening in an argon-filled HCF. We have described numerically a technique for generating tunable sub-two-cycle pulses in the range from 1.5 to 4 μm, which have been also demonstrated experimentally at 1.83 μm center wavelength. In particular, the comparison between experiment and simulations revealed self-steepening as a key process, as well as a significant contribution from higher-order Kerr terms. Compression is simply achieved by propagating the pulse through a FS plate, which exhibits negative GDD in the IR range, after nonlinear propagation in a standard HCF setup. Our numerical simulations show that self-steepening allows a better compression than expected due to SPM only because steepening induces a negative third-order component which partially compensates the positive TOD of FS. Moreover, we have identified the processes involved in the spectral broadening process. Thus, it appears that higher-order Kerr terms have an important impact to adequately fit the experimental results. Moreover, the excellent quantitative agreement of our model with respect to the experiments driven at 1.83 μm allowed us to discuss the optimal parameters for generating sub-two-cycle pulses in the 1.5- to 4-μm range. Such a tunable, few-cycle IR source will be useful in the scope of attosecond pulse generation experiments, where the cutoff frequency of the XUV radiations quadratically depends on the pump wavelength.

ACKNOWLEDGMENTS

This work was supported by the ANR COMOC and the Swiss NSF (Contract Nos. 200021-116198 and 200021-125315). Experiments were carried out at the Advanced Laser Light Source (ALLS) at INRS in Varennes (Canada) and the support of the Canada Foundation for Innovation, the Canadian Institute for Photonic Innovations, the Natural Sciences and Engineering Research Council of Canada, and the Fonds Québécois de la Recherche sur la Nature et les Technologies is greatly acknowledged. We gratefully acknowledge the fruitful discussions with D. M. Villeneuve and Paul Corkum, as well as the help and the time spent on the laser system by François Poitras and Antoine Laramée.

[1] D. Strickland and G. Mourou, Opt. Commun. **56**, 219 (1985).
[2] M. Nisoli, S. Stagira, S. DeSilvestri, O. Svelto, S. Sartania, Z. Cheng, M. Lenzner, C. Spielmann, and F. Krausz, Appl. Phys. B **65**, 189 (1997).
[3] C. P. Hauri, W. Kornelis, F. W. Helbing, A. Heinrich, A. Couairon, A. Mysyrowicz, J. Biegert, and U. Keller, Appl. Phys. B **79**, 673 (2004).
[4] S. Skupin, G. Stibenz, L. Bergé, F. Lederer, T. Sokollik, M. Schnurer, N. Zhavoronkov, and G. Steinmeyer, Phys. Rev. E **74**, 056604 (2006).
[5] P. Béjot, J. Kasparian, and J.-P. Wolf, Phys. Rev. A **78**, 043804 (2008).
[6] M. Nisoli, S. Stagira, S. De Silvestri, O. Svelto, G. Valiulis, and A. Varanavicius, Opt. Lett. **23**, 630 (1998).
[7] X. Gu *et al.*, Opt. Express **17**, 62 (2009).
[8] M. Yamashita, K. Yamane, and R. Morita, IEEE J. Quantum Electron. **12**, 213 (2006).
[9] E. Goulielmakis *et al.*, Science **320**(5883), 1614 (2008).
[10] P. B. Corkum and F. Krausz, Nat. Phys. **3**, 381 (2007).
[11] P. B. Corkum, Phys. Rev. Lett. **71**, 1994 (1993).
[12] B. E. Schmidt *et al.*, Appl. Phys. Lett. (to be published).
[13] L. Bergé, S. Skupin, and G. Steinmeyer, Phys. Rev. A **79**(3), 033838 (2009).
[14] A. Baltuška, M. S. Pshenichnikov, and D. A. Wiersma, Opt. Lett. **23**, 1474 (1998).
[15] M. J. Weber, *Handbook of Optical Materials* (CRC Press, Boca Raton, FL, 2003).
[16] G. P. Agrawal, *Nonlinear Fiber Optics*, 3rd ed. (Academic Press, San Diego, 2001).
[17] V. Loriot, E. Hertz, O. Faucher, and B. Lavorel, Opt. Express **17**, 13429 (2009); **18**, 3011(E) (2010).
[18] W. Ettoumi, Y. Petit, J. Kasparian, and J.-P. Wolf, Opt. Express **18**, 6613 (2010).
[19] G. Genty, P. Kinsler, B. Kibler, and J. M. Dudley, Opt. Express **15**, 5382 (2007).
[20] *Handbook of Optics*, 2nd ed. (McGraw-Hill, Columbus, OH, 1994), Vol. 2.
[21] I. H. Malitson, J. Opt. Soc. Am. **55**, 1205 (1965).
[22] P. Béjot, J. Kasparian, S. Henin, V. Loriot, T. Vieillard, E. Hertz, O. Faucher, B. Lavorel, and J.-P. Wolf, Phys. Rev. Lett. **104**, 103903 (2010).
[23] B. Kibler, J. M. Dudley, and S. Coen, Appl. Phys. B **81**, 337 (2005).